Influence of ancillary ligands and solvents on the nuclearity of Ni–Ln complexes

Jean- Pierre Costes, Sonia Mallet-Ladeira, Laure Vendier, Rémi Maurice, Wolfgang Wernsdorfer

Influence of ancillary ligands and solvents on the nuclearity of Ni–Ln complexes†

Jean-Pierre Costes, *[a] Sonia Mallet-Ladeira,[a] Laure Vendier,[a] Rémi Maurice *[b] and Wolfgang Wernsdorfer *[c]

A Schiff base ligand resulting from the reaction of ovanillin and 2,2-dimethyl-1,3-diaminopropane allows the preparation of hetero-dinuclear $[Ni–Ln]^{3+}$ or -trinuclear $[Ni–Ln–Ni]^{3+}$ complexes. Although empirical parameters for rationalizing the strength of the ferromagnetic Ni–Gd interaction have already been discussed in several papers, no systematic study has been devoted to the control of the nuclearity of such complexes. With the help of structural determinations, we demonstrate the role of solvent and of the nature of ancillary ligands, linked to the Ln ions, in nuclearity. For instance, the presence of one chelating nitrato ligand is already sufficient to impede an increase in the nuclearity, while the replacement of nitrato ligands by chloride anions still yields dinuclear Ni–Ln complexes. This experimental result evidences the role of protic solvents. In contrast, the use of lanthanide salts, soluble in non-protic solvents, allows the isolation of dinuclear $[Ni–Ln]^{3+}$ or trinuclear cationic $[LNi–Ln–NiL]^{3+}$ complexes, depending on the Ni/Ln ratio. A further synthetic step can be overtaken by the reaction of a Ni–Ln complex, soluble in a non-protic solvent, with a LM complex (M = Cu, Zn). By doing so, a heterotrinuclear complex made of three different metal ions, two distinct 3d ions and a 4f one, has been isolated and structurally characterized. Note that the Ni coordination number decreases from 6 to 5 on going from the dinuclear complex to the trinuclear one. Also, the replacement of water molecules by chloride ligands in the hexacoordinate Ni complexes induces a net increase of the positive zero-field splitting parameter D to 20 cm^{-1}, which is supported by *ab initio* calculations. Although the Ni–Ln (Ln = Gd, Tb, Dy) magnetic interactions are ferromagnetic, the corresponding trinuclear complexes are devoid of SMM properties in the absence of an applied magnetic field.

Introduction

The first example of an $S = 9/2$ ferromagnetic ground state for a dinuclear Ni–Gd complex appeared in the literature in 1997.[1] This complex was prepared by use of a Schiff base ligand resulting from the reaction of ovanillin and 2,2-dimethyl-1,3-diaminopropane in which the nickel ion occupies the inner N_2O_2 coordination site and the gadolinium one is coordinated in the larger and outer O_2O_2 site. Three chelating nitrato ancillary ligands complete the Gd coordination sphere and cause electroneutrality of the molecule. Since then, several examples of Ni–Gd complexes have been published with the help of similar or different Schiff bases,[2] tripodal ligands[2p,3] or other ligands.[4] Dinuclear or trinuclear complexes have been characterized but the strength of the ferromagnetic Ni–Gd interaction was always lower than the one reported in the first complex. If parameters able to rationalize the strength of the ferromagnetic Ni–Gd interaction have been previously discussed,[2i,k,n] those involved in the nuclearity of the Ni–Ln complexes built with Schiff base ligands are the subject of the present paper. Their knowledge allows the preparation of heterotrinuclear complexes involving two different transition metal ions along with a lanthanide ion. So complexes resulting from the use of different lanthanide salts, chloride, and triflate, in the presence of protic or non-protic solvents, have been structurally determined. The magnetic properties of these complexes, the zero-field splitting D parameters of the Ni ions, the temperature dependence of their magnetic susceptibilities, and the field dependence of their magnetizations, have also been measured. State-of-the-art *ab initio* calculations complete this work in order to give further insights into the anisotropy of these systems.

[a]*LCC-CNRS, Université de Toulouse, CNRS, 31077 Toulouse, France. E-mail: jean-pierre.costes@lcc-toulouse.fr*
[b]*SUBATECH, UMR CNRS 6457, IN2P3/IMT Atlantique/Université de Nantes, Nantes, France*
[c]*Institu Néel, CNRS, BP 166, 25 Avenue des Martyrs, 38042 Grenoble Cedex 9, France; and Physikalisches Institut and Institute of Nanotechnology, Karlsruhe Institute of Technology, Wolfgang-Gaede-Str. 1, 76131 Karlsruhe, Germany*

Experimental section

Materials

[LNi]·1.75H_2O,[5] (L = *N*,*N*′-2,2-dimethylpropylenedi(3-methoxysalicylideneiminato) ligand), LZn·H_2O,[6] LCu·2H_2O,[7] $[(H_2O)_2NiLEr(NO_3)_3]^{2k}$ and $NiLGd(CF_3SO_3)_3(H_2O)_2$ [5] were prepared as previously described. The $[(H_2O)NiLLn(H_2O)LNi(H_2O)](CF_3SO_3)_3$ complexes were prepared according to the Gd and Eu equivalent compounds with the use of the corresponding $Ln(CF_3SO_3)_3$ starting material (Ln = Gd, Tb, Dy, Y).[2p,5] The metal salts $GdCl_3·6H_2O$ and $YCl_3·6H_2O$ were used as purchased. High-grade solvents (acetone, acetonitrile, dichloromethane, methanol) and distilled water were used for the preparation of the complexes.

Syntheses

$[(H_2O)_2NiLEr(NO_3)(H_2O)_3](NO_3)_2(H_2O)$ (1). $[(H_2O)_2NiLEr(NO_3)_3]$ was dissolved in a minimum amount of water. Diffusion of acetone into the water solution yielded crystals suitable for X-ray analysis. Anal. calcd for $C_{21}H_{36}ErN_5NiO_{19}$ (888.5): C, 28.39; H, 4.08; N, 7.88. Found: C, 27.95; H, 3.96; N, 7.35.

$[Cl_2NiLGd(H_2O)_4]Cl(H_2O)_2$ (2). The addition of $GdCl_3·6H_2O$ (0.18 g, 0.5 mmol) to a stirred suspension of [LNi]·1.75H_2O (0.23 g, 0.5 mmol) in methanol (10 mL) induced dissolution of the nickel complex with colour change. The mixture was stirred at room temperature and the green solution was reduced to half-volume. Slow evaporation yielded crystals suitable for X-ray analysis. Yield: 0.20 g (50%). Anal. calcd for $C_{21}H_{36}Cl_3GdN_2NiO_{10}$ (798.8): C, 31.58; H, 4.54; N, 3.51. Found: C, 31.12; H, 4.31; N, 3.35. IR: 3234l, 1620s, 1562w, 1463s, 1428m, 1392w, 1371w, 1296s, 1219s, 1197w, 1165w, 1099w, 1061m, 966w, 926w, 852w, 779w, 738m, 644w, 618w cm^{-1}.

$[Cl_2NiLY(H_2O)_4]Cl(H_2O)_2$ (3). The replacement of $GdCl_3·6H_2O$ by $YCl_3·6H_2O$ according to the same experimental process yielded crystals suitable for X-ray analysis. Yield: 0.18 g (49%). Anal. calcd for $C_{21}H_{36}Cl_3N_2NiO_{10}Y$ (730.49): C, 34.53; H, 4.97; N, 3.83. Found: C, 34.23; H, 4.74; N, 3.62. IR: 3228l, 1619s, 1562w, 1463s, 1428m, 1392w, 1370w, 1298s, 1219s, 1196w, 1164w, 1098w, 1061m, 966w, 925w, 852w, 779w, 738m, 644w, 619w cm^{-1}.

$[(H_2O)NiLTb(H_2O)LNi(H_2O)](CF_3SO_3)_3$ (4). A mixture of $[L^1Ni]·1.75H_2O$ (0.23 g, 5×10^{-4} mol) and $Tb(CF_3SO_3)_3$ (0.15 g, 2.5×10^{-4} mol) in acetone (15 mL) was stirred for thirty minutes and then filtered off. The solution was concentrated to 5 mL. The addition of CH_2Cl_2 (15 mL) and stirring at room temperature yielded a green precipitate that was filtered off and dried. Yield: 0.26 g (68%). Anal. calcd for $C_{45}H_{54}F_9N_4Ni_2O_{20}S_3Tb$ (1514.42): C, 35.69; H, 3.59; N, 3.70. Found: C, 35.12; H, 3.30; N, 3.61. IR: 3326l, 2956w, 1623s, 1565w, 1472s, 1438m, 1394w, 1368w, 1285s, 1221vs, 1163s, 1078w, 1064m, 1028s, 968m, 925w, 851w, 781w, 743m, 635m cm^{-1}.

$[(H_2O)NiLDy(H_2O)LNi(H_2O)](CF_3SO_3)_3$ (5). This complex was prepared according to the reaction process described above for complex **4**, with the use of $Dy(trifl)_3$ in place of $Tb(trifl)_3$. Yield: 0.30 g (79%). Anal. calcd for $C_{45}H_{54}DyF_9N_4Ni_2O_{20}S_3$ (1517.99): C, 35.61; H, 3.59; N, 3.69. Found: C, 35.09; H, 3.32; N, 3.53. IR: 3328l, 2956w, 1625s, 1565w, 1473s, 1438m, 1394w, 1368w, 1286s, 1223vs, 1166s, 1079w, 1066m, 1028s, 969m, 930w, 852w, 782w, 743m, 637m cm^{-1}.

$[(H_2O)NiLY(H_2O)LNi(H_2O)](CF_3SO_3)_3$ (6). This complex was prepared according to the reaction process described above for complex **4**, with the use of $Y(trifl)_3$ in place of $Tb(trifl)_3$. Yield: 0.24 g (66%). Anal. calcd for $C_{45}H_{54}F_9N_4Ni_2O_{20}S_3Y$ (1444.40): C, 37.42; H, 3.77; N, 3.88. Found: C, 36.95; H, 3.46; N, 3.59. Slow diffusion of dichloromethane into an acetone solution of the isolated precipitate yielded crystals suitable for an X-ray analysis. IR: 3326l, 2957w, 1623s, 1565w, 1472s, 1438m, 1394w, 1368w, 1286s, 1222vs, 1163s, 1079w, 1064m, 1029s, 968m, 930w, 851w, 781w, 743m, 636m cm^{-1}.

$[(H_2O)NiLGd(H_2O)LZn(H_2O)](CF_3SO_3)_3$ (7). *Method a*: NiLGd $(triflate)_3(H_2O)_2$ (0.44 g, 0.42 mmol) and LZn(H_2O) (0.19 g, 0.42 mmol) were mixed in acetone (10 mL), heated and stirred for 10 min, yielding a green solution. The cooled solution was filtered off and concentrated to half-volume. Diffusion of CH_2Cl_2 yielded crystals suitable for X-ray analysis.

Method b: [LNi]·1.75H_2O (0.23 g, 0.5 mmol) and $Gd(trif)_3$ (0.30 g, 0.5 mmol) in acetone (10 mL) were stirred for 30 min, yielding an uncoloured solution that was filtered off. The solution, which turned green after the addition of LZn(H_2O) (0.23 g, 0.5 mmol), was filtered and concentrated to half-volume. Diffusion of CH_2Cl_2 yielded crystals suitable for X-ray. Yield: 0.40 g (55%). Anal. calcd for $C_{45}H_{54}F_9GdN_4NiO_{20}S_3Zn$ (1519.44): C, 35.57; H, 3.58; N, 3.69. Found: C, 35.33; H, 3.38; N, 3.54. IR: 3306l, 2957w, 1624s, 1562w, 1472s, 1437m, 1394w, 1367w, 1284s, 1219vs, 1162s, 1078w, 1063m, 1028s, 967m, 928w, 849w, 781w, 737m, 636m cm^{-1}.

$[(H_2O)NiLY(H_2O)LZn(H_2O)](CF_3SO_3)_3$ (8). This complex was prepared according to method b described above and with the use of $Y(trifl)_3$ in place of $Gd(trifl)_3$. Yield: 0.46 g (63%). Anal. calcd for $C_{45}H_{54}F_9N_4NiO_{20}S_3YZn$ (1451.10): C, 35.25; H, 3.75; N, 3.86. Found: C, 34.92; H, 3.47; N, 3.62. IR: 3302l, 2957w, 1625s, 1563w, 1473s, 1438m, 1394w, 1368w, 1285s, 1219vs, 1163s, 1078w, 1063m, 1028s, 967m, 929w, 849w, 781w, 743m, 636m cm^{-1}.

$[(H_2O)NiLGd(H_2O)LCu](CF_3SO_3)_3$ (9). [LNi]·1.75H_2O (0.23 g, 0.5 mmol) and $Gd(trif)_3$ (0.30 g, 0.5 mmol) in acetone (10 mL) were stirred for 30 min, yielding an uncoloured solution that was filtered off. The solution, which turned green after the addition of LCu·2H_2O (0.24 g, 0.5 mmol), was filtered and concentrated to half-volume. Diffusion of CH_2Cl_2 yielded crystals. Yield: 0.40 g (53%). Anal. calcd for $C_{45}H_{52}CuF_9GdN_4NiO_{19}S_3$ (1499.58): C, 36.04; H, 3.50; N, 3.74. Found: C, 35.69; H, 3.27; N, 3.55. IR: 3319l, 2957w, 1625s, 1566w, 1476s, 1439m, 1394w, 1368w, 1290s, 1226vs, 1167s, 1067m, 1030s, 971m, 929w, 852w, 781w, 743m, 638m cm^{-1}.

$CuLGdLCu(H_2O)_2(CF_3SO_3)_3$ (10). A mixture of $L^1Cu·2H_2O$ (0.24 g, 5×10^{-4} mol) and $Gd(CF_3SO_3)_3$ (0.15 g, 2.5×10^{-4} mol) in acetone (15 mL) was stirred for thirty minutes and then filtered off. The solution was concentrated to 5 mL. The addition of CH_2Cl_2 (15 mL) and stirring at room temperature yielded a green precipitate that was filtered off and dried. Yield: 0.23 g

(62%). Anal. calcd for $C_{45}H_{52}Cu_2F_9GdN_4O_{19}S_3$ (1504.44): C, 35.93; H, 3.48; N, 3.72. Found: C, 35.56; H, 3.29; N, 3.58. IR: 3439l, 2958w, 1623s, 1567w, 1473s, 1438m, 1394w, 1286s, 1223vs, 1160s, 1063m, 1027s, 969m, 930w, 851w, 781w, 741m, 636m cm^{-1}.

Physical measurements

Elemental analyses were carried out at the Laboratoire de Chimie de Coordination Microanalytical Laboratory in Toulouse, France, for C, H, and N. IR spectra were recorded on a Spectrum 100 FT-IR PerkinElmer spectrophotometer using the ATR mode. Magnetic data were obtained with a Quantum Design MPMS SQUID susceptometer. Magnetic susceptibility measurements were performed in the 2–300 K temperature range in a 0.1 T applied magnetic field, and diamagnetic corrections were applied by using Pascal's constants.[8] Isothermal magnetization measurements were performed up to 5 T at 2 K. The magnetic susceptibilities have been computed by exact calculations of the energy levels associated with the spin Hamiltonian through diagonalization of the full matrix with a general program for axial and rhombic symmetries,[9] and the magnetizations with the MAGPACK program package.[10] Least-squares fittings were accomplished with an adapted version of the function-minimization program MINUIT.[11]

Crystallographic data collection and structure determination for (1), (2), (3), and (8)

Crystals were kept in the mother liquor until they were dipped into oil. The chosen crystals were mounted on a Mitegen micromount and quickly cooled down to 180 K. The selected crystals of (**1**) (purple, 0.40 × 0.20 × 0.20 mm^3), (**2**) (green, 0.25 × 0.12 × 0.05 mm^3), (**3**) (green, 0.30 × 0.22 × 0.08 mm^3), and (**8**) (pale green, 0.15 × 0.08 × 0.02 mm^3) were mounted on a STOE IPDS (**1**), a Bruker Kappa APEX II (**2**) or a Xcalibur (**3**, **8**) diffractometer using graphite-monochromated Mo-Kα radiation (λ = 0.71073 Å) and equipped with an Oxford Cryosystems Cryostream Cooler Device. Data were collected at low temperature (180 K). The final unit cell parameters have been obtained by means of least-squares refinements. The structures have been solved by direct methods using SIR92,[12] and refined by means of least-squares procedures on an F^2 with the program SHELXL97[13] included in the software package WinGX version 1.63.[14] Positional parameters of the H atoms of water molecules in (**1**) were obtained from difference Fourier syntheses and verified by the geometric parameters of the corresponding hydrogen bonds. The atomic scattering factors were taken from International Tables for X-Ray Crystallography.[15] All non-hydrogen atoms were anisotropically refined, and in the last cycles of refinement a weighting scheme was used, where weights are calculated from the following formula: $w = 1/[\sigma^2(F_o^2) + (aP)^2 + bP]$ where $P = (F_o^2 + 2F_c^2)/3$. Drawings of molecules are performed with the programs ORTEP32 with 30% probability displacement ellipsoids for non-hydrogen atoms.[16]

Crystal data for 1: $C_{21}H_{36}ErN_5NiO_{19}$, M = 888.52, triclinic, $P\bar{1}$, Z = 2, a = 9.8381(11), b = 12.6145(16), c = 12.8061(15) Å, α = 89.022(15)°, β = 86.952(14)°, γ = 73.975(14)°, V = 1525.3(3) $Å^3$, 15 153 collected reflections, 5588 unique reflections (R_{int} = 0.0677), R = 0.0347, R_w = 0.0886 for 5185 contributing reflections [$I > 2\sigma(I)$]. CCDC 1877427.†

Crystal data for 2: $C_{21}H_{36}Cl_3GdN_2NiO_{10}$, M = 798.83, orthorhombic, $Pca2_1$, Z = 4, a = 8.8734(3), b = 16.4237(7), c = 20.2362(8) Å, $\alpha = \beta = \gamma$ = 90°, V = 2949.1(2) $Å^3$, 112 448 collected reflections, 13 037 unique reflections (R_{int} = 0.0251), R = 0.0185, R_w = 0.0372 for 12 081 contributing reflections [$I > 2\sigma(I)$]. CCDC 1877430.†

Crystal data for 3: $C_{21}H_{36}Cl_3N_2NiO_{10}Y$, M = 730.49, orthorhombic, $Pca2_1$, Z = 4, a = 8.8025(2), b = 16.3713(4), c = 20.1951(5) Å, $\alpha = \beta = \gamma$ = 90°, V = 2910.28(12) $Å^3$, 20 707 collected reflections, 5928 unique reflections (R_{int} = 0.0346), R = 0.0199, R_w = 0.038 for 5337 contributing reflections [$I > 2\sigma(I)$]. CCDC 1877429.†

Crystal data for 8: $C_{47}H_{58}Cl_4F_9N_4NiO_{20}S_3YZn$, M = 1620.94, orthorhombic, $P2_1/c$, Z = 4, a = 16.9580(4), b = 16.2440(4), c = 24.3930(6) Å, $\alpha = \gamma$ = 90, β = 104.880(2)°, V = 6494.1(3) $Å^3$, 58 205 collected reflections, 15 697 unique reflections (R_{int} = 0.0715), R = 0.059, R_w = 0.1414 for 10 102 contributing reflections [$I > 2\sigma(I)$]. CCDC 1877426.†

Calculations

All calculations have been performed with the ORCA program.[17] A similar computational approach to the one used in previous papers is followed.[2m,18] The computational strategy is based on a two-step approach, in which the relativistic spin–orbit coupling (SOC) term is introduced *a posteriori*.[19] In the second step of the calculation, the $\mathbf{E}_{el} + \mathbf{H}_{SOC}$ matrix is diagonalised on the basis of the M_S components of the previously determined spin–orbit-free (SOF) states (here, the SOF states are actually non-relativistic states; in other words, scalar relativistic effects are neglected, as in previous work).[2m,18] Note that $\mathbf{H}_{SOC}$ is computed *via* a mean-field approximation of the SOC operator.[20] In the first step of the calculation, the SOF states are computed at the state-average complete active space self-consistent field (SA-CASSCF) level. The "electronic" energies, corresponding to the elements of the $\mathbf{E}_{el}$ diagonal matrix, may be either directly the SA-CASSCF energies, or the more correlated N-electron valence state second-order perturbation theory (NEVPT2) ones,[21] with the SA-CASSCF wave functions serving as (reference) zeroth-order wave functions. The D and E ZFS parameters are extracted from the SOC energies and wave functions *via* the so-called effective Hamiltonian theory,[22] within the Des Cloizeaux fashion[23] (the projected states are symmetrically orthogonalized – Löwdin's scheme). This approach, initially proposed for treating single-ion anisotropies,[24] has been widely applied to a wide range of mononuclear and binuclear complexes, even with two "active" magnetic sites (see ref. 25 and 26, and references therein). With the NEVPT2 electronic energies, the ZFS parameters are usually found in good agreement with those of the experiment for mononuclear transition metal complexes. The molecular structure of **3** has been extracted from the experimental X-ray structures by simply carving out the molecular unit from the

crystal structure. The ZFS has been computed only for this system to confirm the experimental occurrence of a large single-ion anisotropy for the nickel(II) ion that occurs in this binuclear yttrium(III)–nickel(II) complex that displays apical chlorine ligands. Basis sets[27] of two different sizes were used, a "standard" one with the Y[8s6p5d1f] ("def2-TZVP"), Ni[6s4p4d1f] ("def2-TZVP"), Cl[5s4p2d] ("def2-SVPD"), O[4s3p2d] ("def2-SVPD"), N[4s2p2d] ("def2-SVPD"), C[3s2p1d] ("def2-SVP") and H[2s] ("def2-SV") contractions and an "extended" one consisting of the same contractions except Ni [6s5p4d2f1g] ("def2-TZVPP"), Cl[5s5p2d1f] ("def2-TZVP"), O[5s3p2d1f] ("def2-TZVP") and N[5s3p2d1f] ("def2-TZVP"). With the "extended" basis set, the description of the "central" ion (the nickel one) and its first-coordination-sphere atoms (Cl, O and N) are notably improved. The complete d^8 manifold was considered, *i.e.* 10 spin-triplet and 15 spin-singlet SOF states, as in previous work.[2m,18]

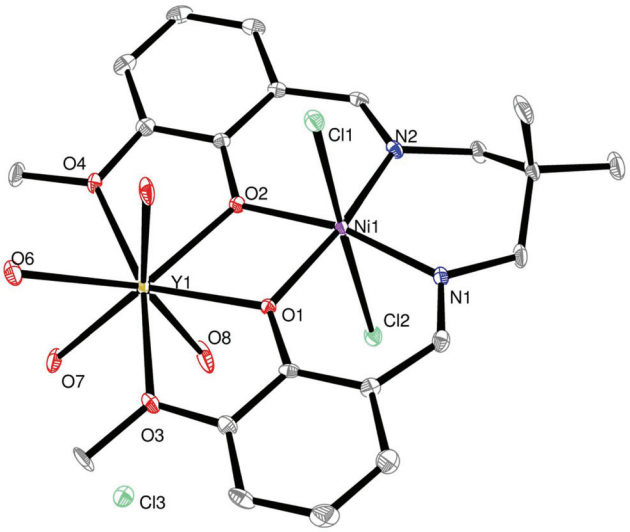

Fig. 2 Plot of complex **3** with ellipsoids drawn at the 30% probability level with partial atom numbering and H atoms omitted for clarity. Selected bond lengths (Å) and angles (°): Ni–N1 2.014(3), Ni–N2 1.998(3), Ni–O1 1.999(2), Ni–O2 2.013(2), Ni–Cl1 2.4980(9), Ni–Cl2 2.767(1), Y–O1 2.301(2), Y–O2 2.285(2), Y–O3 2.417(2), Y–O4 2.430(2), Y–O5 2.313(2), Y–O6 2. 364(2), Y–O7 2. 2.331(2), Y–O8 2.307(3), Ni···Y 3.4988(5) Å; Ni O1 Y 108.73(9), Ni O2 Y 108.82(9), O1 Y O2 65.75(7)°.

Results

Structural analysis

The crystallographic data of complexes **1**, **2**, **3** and **8** appear in the Experimental section while selected bond lengths and angles are collated in the corresponding figure captions. The three heterodinuclear Ni–Ln complexes **1–3** reported in Fig. 1 (complex **1**), Fig. S1† (complex **2**) and Fig. 2 (complex **3**) present common features. The Ni(II) and Ln(III) ions are doubly bridged by the deprotonated phenoxo oxygen atoms of the Schiff base ligand, with these four atoms defining the central NiO_2Ln core of each molecule, which is practically planar for complexes **2** and **3**, with dihedral angles of 1.5(1) and 1.8(1)° respectively. A larger dihedral angle (6.1(1)°) is observed for complex **1**. The Ni ions occupy the inner coordination site, surrounded by the four N_2O_2 donor atoms of the ligand in the equatorial position and by two water oxygen atoms (complex **1**) or two chloride anions (complexes **2** and **3**) in the axial position. The axial Ni–O bond lengths (2.089(3)–2.209(3) Å) are larger than the basal Ni–O bond lengths (1.999(2)–2.025(3) Å), while the Ni–Cl bond lengths are larger (2.4980(9)–2.767(1) Å). The Ln ions are coordinated to the outer O_2O_2 coordination site, linked to the two phenoxo and two methoxy oxygen atoms of the ligand. The Ln coordination sphere is completed by a chelating nitrato anion and three water molecules for complex **1** and by four water molecules for complexes **2** and **3**, thus yielding nine (**1**) or eight-coordinate Ln ions (**2**, **3**). The intramolecular Ni–Ln distances depend on the Ln ions, varying from 3.5294(3) (Ln = Gd) to 3.4988(5) (Ln = Y) and to 3.4632(8) (Ln = Er) Å. The large separations between metal ions belonging to neighbouring molecules preclude any significant intermolecular interaction of magnetic nature.

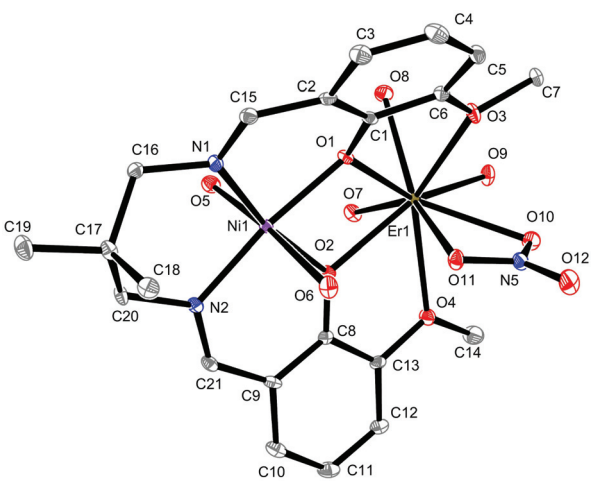

Fig. 1 Plot of complex **1** with ellipsoids drawn at the 30% probability level with partial atom numbering and H atoms omitted for clarity. Selected bond lengths (Å): Ni–N1 2.001(4), Ni–N2 2.019(3), Ni–O1 2.025(3), Ni–O2 1.999(3), Ni–O5 2.089(3), Ni–O6 2.209(3), Er–O1 2.291(3), Er–O2 2.301(3), Er–O3 2.485(3), Er–O4 2.536(3), Er–O7 2.323(3), Er–O8 2.373(3), Er–O9 2.304(3), Er–O10 2.522(3), Er–O11 2.493(3), Ni···Er 3.4632(8) Å.

The structural determination of complex **8** evidences the existence of a trinuclear cationic Ni–Y–Zn complex with three triflate anions acting as counter ions, as shown in Fig. 3. Complex **8** crystallizes in the monoclinic $P2_1/c$ space group. The main difference in the previously described dinuclear Ni–Ln complexes comes from the coordination of the Ln ions to NiL and ZnL entities, so that the Ln coordination sphere is nine-coordinate, linked to the eight oxygen atoms coming from these NiL or ZnL units, and to one water molecule. The Ni or Zn ions are now five-coordinate, with a unique water molecule linked in the axial position. Note that the three water

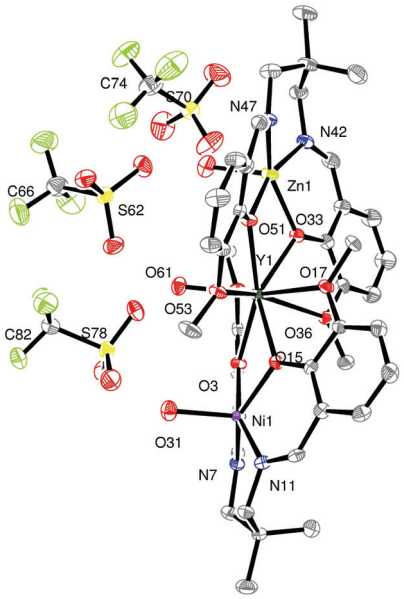

Fig. 3 Plot of complex **8** with ellipsoids drawn at the 30% probability level with partial atom numbering and H atoms omitted for clarity. Selected bond lengths (Å) and angles (°): Ni–N7 2.037(4), Ni–N11 2.028(4), Ni–O3 2.011(3), Ni–O31 2.013(4), Ni–O15 2.094(3), Zn–N42 2.019(4), Zn–N47 2.025(4), Zn–O33 2.047(3), Zn–O51 2.007(3), Zn–O60 2.000(4), Y–O3 2.388(3), Y–O15 2.299(3), Y–O17 2.511(3), Y–O28 2.600(3), Y–O33 2.301(3), Y–O36 2. 503(3), Y–O51 2. 2.374(3), Y–O53 2.588(3), Y–O61 2.276(3), Ni···Y 3.5530(6), Zn···Y 3.5238(7) Å; Ni O3 Y 107.44(12), Ni O15 Y 107.84(11), O3 Y O15 64.44(10)°, Zn O33 Y 108.15(12), Zn O51 Y 106.81(12), O33 Y O51 64.08(10)°.

molecules coordinated to each metal ion point in the same direction and that the equatorial and axial Ni–O and Zn–O bond lengths are comparable (2.011(3)–2.094(3) Å against 2.013(4) Å and 2.007(3)–2.047(3) against 2.000(4) Å, respectively). The LNi or LZn moieties take an umbrella form with the water molecule pointing above while the six-membered diamino rings are in a chair conformation.[5] The related intramolecular Ni···Y and Zn···Y separations are respectively equal to 3.5530(6) and 3.5238(7) Å. The dihedral angles between the two MO_2Ln cores (M = Ni or Zn) are equal to 20.74(1) and 21.25(1)° respectively, with the angle between the two OYO planes being equal to 59.00(1)°. Nevertheless, the Ni···Y···Zn centres can be considered as aligned, with a Ni···Y···Zn angle of 176.91(2)°. Although hydrogen bonds involving the water molecules and the non-coordinated triflate anions are present, the different trinuclear units are well isolated from each other, with intermolecular Ni···Ni or Ni···Zn distances of 9.626(1) and 8.577(1) Å and a Y···Y distance of 9.931(1) Å.

Analysis of the Ln coordination spheres with the "SHAPE" program[28] indicates that in the trinuclear complex **8** the 9-coordinate sphere is far from the regular spherical tricapped trigonal prism or spherical capped square antiprism, whereas the latest environment can be retained in complex **1**. The 8-coordinate Ln ions in complexes **2** and **3** are not far from the regular triangular dodecahedron (see Table S1 in the ESI†).

Magnetic properties

The magnetic susceptibilities of the different complexes have been measured in the 2–300 K temperature range under an applied magnetic field of 0.1 T. Thermal variation of the $\chi_M T$ product for complex **3**, in which the Ni ion is the only magnetically active center, is displayed in Fig. 4. At 300 K $\chi_M T$ is equal to 1.21 $cm^3\ mol^{-1}$ K and it remains constant up to 40 K before following an abrupt decrease to 0.17 $cm^3\ mol^{-1}$ K at 2 K. The magnetic susceptibility has been computed by exact calculation of the energy levels through diagonalization of the full energy-matrix with a Hamiltonian introducing an axial zero field splitting term for Ni, $H = D_{Ni}S_z^2$. The best fit (solid line, Fig. 4) yields the following data, $D_{Ni} = 19.9\ cm^{-1}$, $g = 2.20$ with an R factor equal to 1.5×10^{-5}, $R = \sum[(\chi_M T)^{obs} - (\chi_M T)^{calc}]^2 / \sum[(\chi_M T)^{obs}]^2$. In order to check the validity of these results, the Magpack program has been used to fit the experimental magnetization curve at low temperature. The best simulation reported in Fig. S2† (diamonds) necessitates introduction of a low rhombic E value ($E_{Ni} = 0.3 \times 10^{-3}\ cm^{-1}$).

To support the occurrence of a large and positive D value for complex **3**, *ab initio* calculations have been performed, in which $\mathbf{H} = \mathbf{E}_{el} + \mathbf{H}_{SOC}$ is diagonalised in the second step of the calculation, and for which $\mathbf{E}_{el}$ either corresponds to the SA-CASSCF energies or the NEVPT2 ones (see Table 1). As can

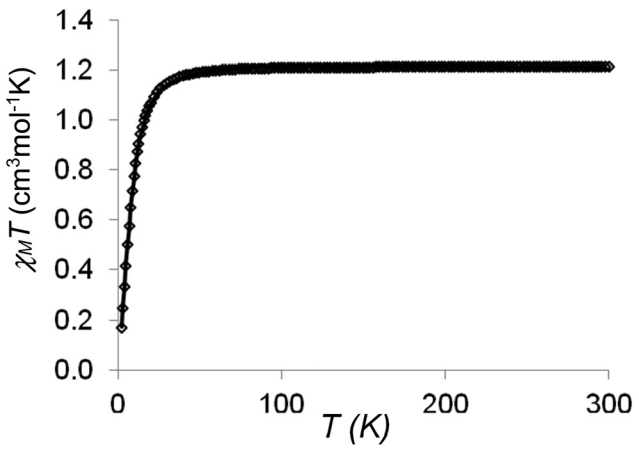

Fig. 4 Temperature dependence of the $\chi_M T$ product for complex **3** at 0.1 T applied field. The solid line corresponds to the best data fit (see the text).

Table 1 *Ab initio* ZFS parameters D and E (cm^{-1}) for complex **3**, computed with the SA-CASSCF or NEVPT2 energies (SO-CASSCF or SO-NEVPT2, respectively) and with a "standard" basis set and with an "extended" one (see the Experimental section for details)

	"Standard" basis set		"Extended" basis set	
Method	D	E	D	E
SO-CASSCF	28.1	2.9	27.4	2.9
SO-NEVPT2	18.5	2.1	17.9	2.0

be seen in this table, the use of the NEVPT2 electronic energies leads to a significant improvement of the ZFS parameters independent of the used basis set, leading in principle to more accurate values. However, the use of the "extended" basis set, for which additional contractions and polarization functions are notably used to describe the nickel(II) ion and the atoms belonging to its first coordination sphere, does not lead to any remarkable change in the computed values. Therefore, it is concluded that the computed values converge with respect to the basis set size at values around 18 cm^{-1} and 2 cm^{-1} for D and E, respectively, *i.e.* to a D value in good agreement with that of the experiment, and a quite overestimated E value (with respect to experiment), as in previous work.[2m,18] This result confirms the occurrence of a large and positive D value in **3**.

The $\chi_M T$ behavior of complex **2** (Fig. 5), where Ni and Gd are magnetically active ions, is quite different. First we observe a slight increase from 300 K (9.29 cm^3 mol^{-1} K) to 40 K (10.30 cm^3 mol^{-1} K), followed by a sharp increase up to 10 K (11.29 cm^3 mol^{-1} K) and eventually a sharp decrease to 9.99 cm^3 mol^{-1} K at 2 K. In view of the previous result, a Hamiltonian introducing an axial zero-field splitting for Ni, $H = -J_{NiGd}(S_{Ni}\cdot S_{Gd}) + D_{Ni}S_z^2$ is used. The fit gives J_{NiGd} = 3.6 cm^{-1}, D_{Ni} = 20.0 cm^{-1}, g = 2.03, and E_{Ni} = 1.3 cm^{-1} with R = 2.0×10^{-5}. A good simulation of the experimental magnetization with the Magpack program and the above parameters confirms their validity (Fig. 6).

A similar study has been conducted for the trinuclear complexes. The first to be studied is complex $[(H_2O)NiLY(H_2O)LZn(H_2O)](CF_3SO_3)_3$ (**8**) (Fig. S3†) in which the Ni ion is the only one to be active, so that a behavior similar to that of complex **3** is expected. At 300 K $\chi_M T$, which is equal to 1.03 cm^3 mol^{-1} K, slightly increases to 1.10 cm^3 mol^{-1} K at 40 K before following an abrupt decrease to 0.15 cm^3 mol^{-1} K at 2 K. Now the best fit yields D_{Ni} = 21.4 cm^{-1}, g = 2.14, E_{Ni} = 0.2×10^{-3} cm^{-1} with an R factor equal to 2×10^{-5}. Note that a temperature-independent parameter (TIP = -0.4×10^{-3}) is needed to correct the slight increase from 300 to 40 K. A good simulation of the experimental magnetization with the Magpack program and the above parameters indicates that we are dealing with the expected complex **8** in which Ni and Zn ions are present, the Ni ion being the only one to be magnetically active (Fig. S4†).

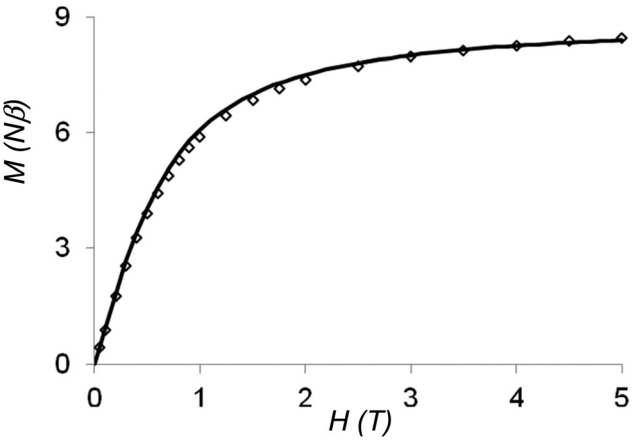

Fig. 6 Field dependence of magnetization for complex **2**. The solid line corresponds to the best data fit (see the text).

In complex $[(H_2O)NiLY(H_2O)LNi(H_2O)](CF_3SO_3)_3$ (**6**), $\chi_M T$ is constant and equal to 2.33 cm^3 mol^{-1} K from 300 to 50 K, where it starts to decrease in order to take a value of 0.33 cm^3 mol^{-1} K at 2 K. Now the situation is complicated by a possible Ni–Ni interaction through the Y ion. If we do not take into account the Ni–Ni interaction, the Hamiltonian $H = D(S_z^2{}_{Ni1} + S_z^2{}_{Ni2})$ yields $D_{Ni1} = D_{Ni2}$ = 23.0 cm^{-1}, g = 2.16 with R = 1.5×10^{-5}, a value confirmed by the simulation of the experimental magnetization curve at low temperature (Fig. 7).

A fit with the Hamiltonian $H = -J_{NiNi}(S_{Ni1}\cdot S_{Ni2}) + D(S_z^2{}_{Ni1} + S_z^2{}_{Ni2})$ gives a weak antiferromagnetic interaction J_{NiNi} = −0.32 cm^{-1}, a slightly lower D_{Ni} term, $D_{Ni1} = D_{Ni2}$ = 18.8 cm^{-1},

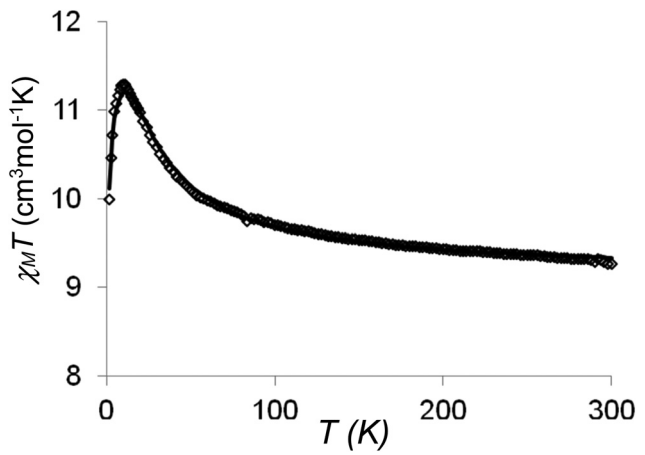

Fig. 5 Temperature dependence of the $\chi_M T$ product for complex **2** at 0.1 T applied field. The solid line corresponds to the best data fit (see the text).

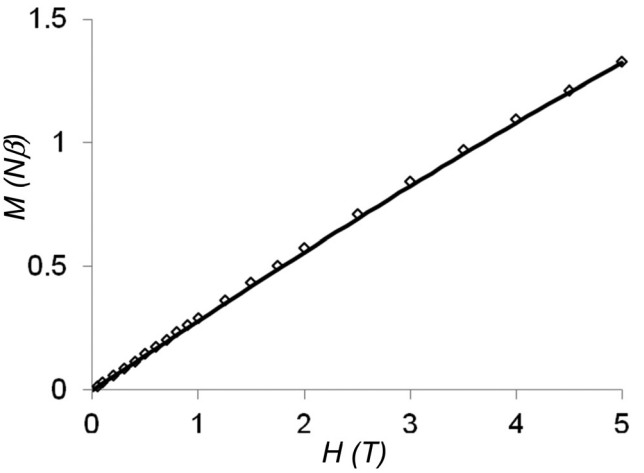

Fig. 7 Field dependence of magnetization for complex **6**. The solid line corresponds to the best data fit (see the text).

$g = 2.16$, $E_{Ni} = 0.34$ cm^{-1} with $R = 2.5 \times 10^{-5}$ (Fig. S5†). To date it has been difficult to tell which is the best solution for we have no proof confirming the presence of a Ni–Ni interaction. Nevertheless, it is clear that the D_{Ni} value is again large, around 20 cm^{-1}. We will see later that micro-SQUID data confirm the presence of intramolecular Ni–Ni interactions and that the second hypothesis has to be retained.

The trinuclear complex $[(H_2O)NiLGd(H_2O)LZn(H_2O)](CF_3SO_3)_3$ (**7**) behaves as the dinuclear complex **2**, with the Zn ion being diamagnetic. From 300 to 100 K, $\chi_M T$ is constant with a 9.43 cm^3 mol^{-1} K value, and then it increases to 10.33 cm^3 mol^{-1} K at 7 K, followed by a further increase to 10.77 cm^3 mol^{-1} K at 2 K (Fig. 8). From 300 to 7 K, this complex can be fitted with the Hamiltonian used for complex **2** while a supplementary zJ term is needed to fit the experimental curve up to 2 K. The final result gives $J_{NiGd} = 1.0$ cm^{-1}, $D_{Ni} = 15.0$ cm^{-1}, $g = 2.04$, and $zJ = 0.9 \times 10^{-2}$ cm^{-1} with $R = 0.3 \times 10^{-5}$. These values allow a good simulation of magnetization at low temperature when the ZFS D_{Ni} term is retained (Fig. S6†).

The complex $[(H_2O)NiLGd(H_2O)LCu](CF_3SO_3)_3$ (**9**) possesses three different magnetic active metal ions. $\chi_M T$ increases slightly from 300 K (9.90 cm^3 mol^{-1} K) to 50 K (11.11 cm^3 mol^{-1} K), followed by a sharp increase up to 10 K (12.98 cm^3 mol^{-1} K) and eventually a weak decrease to 12.80 cm^3 mol^{-1} K at 2 K (Fig. 9). The value at 300 K agrees with the expected value corresponding to non-interacting Ni, Cu and Gd ions (9.50 cm^3 mol^{-1} K). A fit involving the Hamiltonian $H = -J_{NiGd}(S_{Ni}\cdot S_{Gd}) - J_{CuGd}(S_{Cu}\cdot S_{Gd}) + D_{Ni}S_z^2$ furnishes the following parameters, $J_{CuGd} = 10.5$ cm^{-1}, $J_{NiGd} = 1.30$ cm^{-1}, $D_{Ni} = 14.5$ cm^{-1}, and $g = 2.04$ with $R = 0.2 \times 10^{-5}$. These parameters allow a correct simulation of magnetization at low temperature (Fig. S7†).

The J_{CuGd} value is similar to the largest value found in heterodinuclear Cu–Gd complexes.[29] In order to validate this result, the trinuclear $CuLGdLCu(H_2O)_2(CF_3SO_3)_3$ complex (**10**) has been studied. The $\chi_M T$ variation looks like the previous one (Fig. 10), with values going from 8.40 cm^3 mol^{-1} K at 300 K, instead of an expected value of 8.62 cm^3 mol^{-1} K for non-interacting Cu and Gd ions, to 12.08 cm^3 mol^{-1} K. A fit using the Hamiltonian $H = -J_{CuGd}(S_{Cu1}\cdot S_{Gd} + S_{Cu2}\cdot S_{Gd})$ gives $J_{CuGd} = 6.64$ cm^{-1} and $g = 1.98$ with $R = 3.0 \times 10^{-5}$. Note that a supplementary zJ term is needed ($zJ = 0.32 \times 10^{-2}$ cm^{-1}) to fit the last experimental points near 2 K. These parameters simulate nicely the magnetization curve at low temperature (Fig. S8†).

We also report in the ESI (Fig. S9 and S10†) the $\chi_M T$ curves for the $[(H_2O)NiLTb(H_2O)LNi(H_2O)](CF_3SO_3)_3$ and $[(H_2O)NiLDy(H_2O)LNi(H_2O)](CF_3SO_3)_3$ complexes (**4**) and (**5**). $\chi_M T$ for (**4**) is equal to 14.5 cm^3 mol^{-1} K at 300 K, goes through a

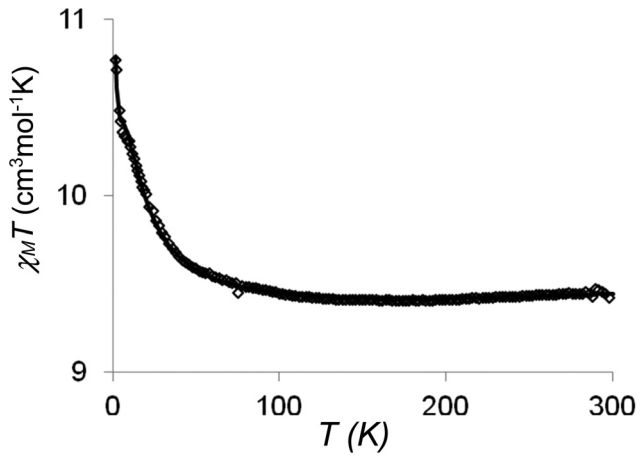

Fig. 8 Temperature dependence of the $\chi_M T$ product for complex **7** at 0.1 T applied field. The solid line corresponds to the best data fit (see the text).

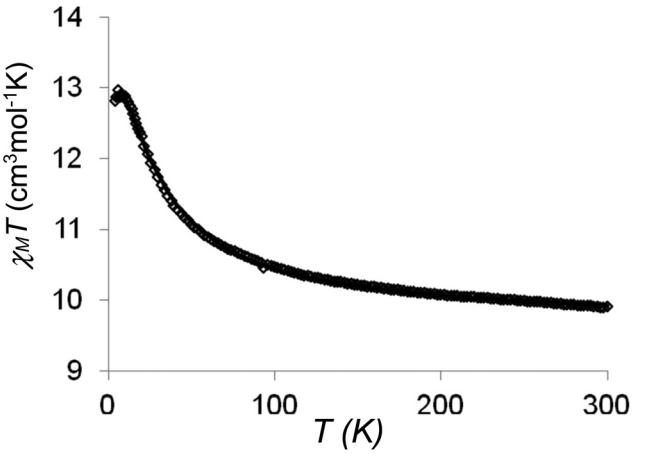

Fig. 9 Temperature dependence of the $\chi_M T$ product for complex **9** at 0.1 T applied field. The solid line corresponds to the best data fit (see the text).

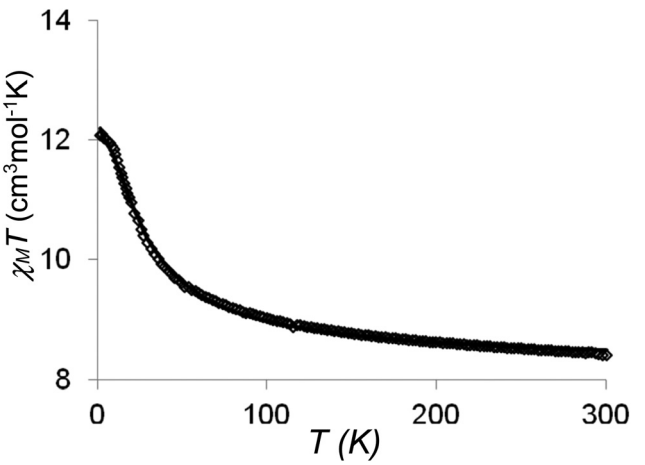

Fig. 10 Temperature dependence of the $\chi_M T$ product for complex **10** at 0.1 T applied field. The solid line corresponds to the best data fit (see the text).

maximum of 16.93 cm^3 mol^{-1} K at 11 K and decreases to 15.12 cm^3 mol^{-1} K at 2 K. A similar behavior, starting at 16.5 cm^3 mol^{-1} K at 300 K, going to a maximum of 18.84 cm^3 mol^{-1} K at 11 K and decreasing to 16.64 cm^3 mol^{-1} K at 2 K, is observed for (**5**). The $\chi_M T$ values at 300 K correspond to the expected values for non-interacting ions, respectively, 14 and 16.37 cm^3 mol^{-1} K for (**4**) and (**5**). The $\chi_M T$ increase below 60 K supports ferromagnetic Ni–Tb and Ni–Dy interactions. The field dependence of magnetizations (Fig. S11 and S12†) confirm the occurrence of ferromagnetic interactions but saturation is not reached, and is far from the expected values, $7.5N\beta$ instead of $11N\beta$ for (**4**) and $7.3N\beta$ instead of $12N\beta$ for (**5**). In order to find out whether compounds (**4**) and (**5**) show SMM behaviour, we performed alternating current (ac) susceptibility measurements in the 2–10 K range using a MPMS SQUID magnetometer with a zero dc field and a 3 Oe ac field oscillating at 10–1000 Hz. No out of phase susceptibility signal was observed in the absence of an applied magnetic field for (**5**) while the onset of an out-of-phase signal is seen above 2 K for (**4**). This is not really surprising if we remember that the dinuclear $[(H_2O)_2NiLLn(NO_3)_3]$ complexes are devoid of such signals in the absence of an applied magnetic field.[2o] The single-crystal magnetizations of these complexes, along with the equivalent trinuclear $[(H_2O)NiLGd(H_2O)LNi(H_2O)](CF_3SO_3)_3$,[2p] were studied with a micro-SQUID array as a function of applied field in the 0.04–5 K range.[30] For the three complexes the measurements at 0.04 K revealed hysteresis loops that collapse at the zero-field (Fig. S13–S15†). Although large-spin ground states are expected in these complexes, due to ferromagnetic Ni–Tb, Ni–Dy, and Ni–Gd interactions, a uniaxial and negative magnetoanisotropy is not present. We can imagine that the Ni ions, with their positive anisotropy, play an inefficient role that is not overthrown by the introduction of anisotropic Tb or Dy ions. Eventually an efficient zero-field quantum tunneling of magnetization impedes our complexes to be interesting single-molecule magnets. The hysteresis loops of the trinuclear Ni–Gd–Ni complex shows a "double-S-like" curve (Fig. S13†), which is characteristic of small antiferromagnetic interactions, that can be attributed here to the intramolecular Ni–Ni interaction.

Discussion

The structural determination of complex $[(H_2O)_2NiLEr(NO_3)(H_2O)_3](NO_3)_2(H_2O)$ (**1**) does confirm that the dinuclear Ni–Ln complexes made with the dideprotonated *N*,*N*′-2,2-dimethylpropylenedi(3-methoxysalicylideneiminato) Schiff base ligand are stable in an aqueous medium. Nevertheless, the erbium coordination sphere of the dissolved starting complex and of the recovered crystallized complex presents some differences. If the four oxygen atoms of the ligand are coordinated to the Er ion in the two complexes, three chelating nitrato anions complete the coordination sphere in the initial complex[2k] while only one is observed in the recrystallized entity, with the Er coordination sphere being completed to nine by three water molecules. This result is in complete agreement with conductivity measurements. In acetone, the $[(H_2O)_2NiLEr(NO_3)_3]$ complex is a non-electrolyte (Λ_M = 10.2 Ω^{-1} cm^2 mol^{-1}) while it becomes a 2/1 electrolyte in methanol (Λ_M = 167.6 Ω^{-1} cm^2 mol^{-1}), which confirms that the Ni–Er complex is stable in a solution of protic solvent and that a nitrato anion is coordinated to the Er ion in solution. This must be the reason why it is impossible to obtain trinuclear $[LNi–Ln–NiL]^{3+}$ complexes in the presence of nitrato anions. It becomes possible to understand the surprising magnetic behavior of the previously published $(LNi)_2Gd(NO_3)_3(H_2O)_2$ entity,[5] which is not a trinuclear LNi–Ln–NiL compound but a new example of a metal complex as a second-sphere ligand.[31] Although its structural determination is unknown, the magnetic results and our present observation allow us to bring forward a $[NiL][(H_2O)_2NiLGd(NO_3)_3]$ formulation, with a water molecule linked to the Ni ion being hydrogen-bonded to the oxygen atoms of the free outer coordination site of the NiL complex.

Reacting $LNi{\cdot}1.75H_2O$ with lanthanide chloride salts in methanol still yielded heterodinuclear complexes formulated $[Cl_2NiLLn(H_2O)_4]Cl(H_2O)_2$ (Ln = Gd (**2**), Y (**3**)) in which two chloride anions enter the Ni coordination sphere in place of the water molecules present in (**1**). The Ln ions are eight-coordinate, linked to the four oxygen atoms of the ligand and to four water molecules, and a third free chloride anion ensuring electroneutrality. A change of the Ni/Ln ratio from 1/1 to 2/1 did not allow isolation of trinuclear Ni–Ln–Ni entities. These structural determinations evidence the role of protic solvents, able to impede the coordination of a second NiL entity in the Ln coordination sphere. In contrast, lanthanide triflates are soluble in non-protic solvents. Working in acetone, it is possible to isolate heterodinuclear $(H_2O)_2NiLGd(CF_3SO_3)_3$ [1,2k] and heterotrinuclear $[(H_2O)NiLLn(H_2O)LNi(H_2O)](CF_3SO_3)_3$ complexes,[2p] according to the LNi/Ln ratio (Ln = Gd, Eu). We completed the series of trinuclear complexes with Ln = Tb, Dy, Y. The structural determinations indicate that the Ni coordination spheres become pentacoordinate with only a water molecule in the apical position for the trinuclear complexes, instead of being hexacoordinate in the dinuclear ones. We can also remark that the three water molecules coordinated to the metal ions, two from each Ni ion and the third one from the Ln ion, are roughly oriented in the same direction.

Furthermore, as we demonstrated above that the Ni–Ln complexes are stable even in protic solvents, working in acetone should yield complexes involving two different 3d ions around the Ln ion. Indeed the addition of LZn or LCu compounds to $(H_2O)_2NiLLn(CF_3SO_3)_3$ complexes allows the preparation of complexes (**7**–**9**), which are genuine Ni–Gd–Zn, Ni–Y–Zn and Ni–Gd–Cu complexes. Structural determinations confirm that the Ni and Zn ions are pentacoordinate, as in the Ni–Ln–Ni[2n,p] or Zn–Ln–Zn[32] complexes. The starting heterodinuclear triflate Ni–Ln complexes are faint-colored, as the nitrate equivalents,[2k,5] while the resulting trinuclear ones are green complexes, with the color change coming from the Ni coordination sphere, going from hexa- to pentacoordination.

To date, we have noticed the negative role of nitrate anions and protic solvents in the preparation of trinuclear Ni–Ln–Ni complexes. We have recently published some complexes resulting from the reaction of dinuclear $[(H_2O)_2NiLLn(NO_3)_3]$ entities with highly charged anionic species such as metallocyanates $W(CN)_8^{3-}$ or $Co(CN)_6^{3-}$ that seem to overrule our above conclusions.[2o,33] If trinuclear W–Ni–Ln or hexanuclear $[W–Ni–Ln]_2$ and $[Co–Ni–Ln]_2$ have been structurally characterized, we must recall that these metallocyanates are able to coordinate the Ni ion and even the Ln ion,[34] thus impeding solvent coordination and repelling nitrate anions.

Concerning magnetic anisotropy, the $[Cl_2NiLY(H_2O)_4]Cl(H_2O)_2$ complex presents strong analogies with the previously studied $[(H_2O)_2NiLY(NO_3)_3]$ one.[2m,18] *Ab initio* calculations confirmed that the *Z* axis, which is a hard axis of magnetization, corresponds to the elongation axis of the Ni ion while the Ni–Y^{III} orientation corresponds to another magnetic axis, actually to the easy axis of magnetization (here, it corresponds to the *Y* axis in both spread conventions, *i.e.* with a positively defined *E* or a positively defined *E*/*D* ratio, since *D* is positive). Note that Abragam and Bleaney reported decades ago that axially elongated 6-coordinate Ni^{II} complexes are characterized by positive D_{Ni} values.[35] Therefore, the replacement of the water molecules axially linked to the Ni ion in $[(H_2O)_2NiLY(NO_3)_3]$ by axial chloride anions, as in the $[Cl_2NiLLn(H_2O)_4]Cl(H_2O)_2$ complexes, leads to a increase of the positive D_{Ni} zero-field splitting term from 10 to around 20 cm^{-1}, while the position of the magnetic anisotropy axes remains practically unchanged. As expected (though there may exist a few exceptions to this[2m,36]), the positions of the first-coordination sphere atoms around the Ni ion rule the zero-field splitting (ZFS) and are key ingredients for controlling the low-temperature magnetic behavior of these complexes.

In the case of pentacoordinate Ni in the Ni–Y complexes, D_{Ni} zero-field splitting terms can be positive or negative, depending on geometrical features.[2m,18,37] When negative D_{Ni} terms are observed, the ZFS is dominated by the electrostatic effect of the Y^{III} ion that belongs to the second coordination sphere of the Ni ion. Such a situation implies a shorter Ni···Y distance, along with a less important axial elongation of the Ni coordination sphere. Furthermore, from the magnetic point of view, the $\chi_M T$ decrease at low temperature is less marked compared to that in complexes involving negative D_{Ni} values.[2m,18] The structural parameters of our trinuclear Ni–Y–Zn complex indicate a lengthening of the Ni···Y distances (3.553(7) Å) and a shortening of the axial Ni–O(water) bonds (2.014(4) Å). The low temperature $\chi_M T$ values are respectively equal to 0.33 and 0.15 $cm^3\ mol^{-1}$ K for (**6**) and (**8**), so that positive *D* terms are expected in these trinuclear complexes. The quality of the fits, $\chi_M T$ *vs.* *T* and *M* *vs.* *H* (see Fig. 7 and S3–S5†), do agree with these solutions. Note that we have been unable to fit these curves with negative D_{Ni} values and that the D_{Ni} parameters found in these trinuclear complexes are in good agreement with the fit appearing in the literature for the $[(H_2O)NiLGd(H_2O)LNi(H_2O)](CF_3SO_3)_3$ complex.[2n] Therefore, we are confident in the fitted values, and chose not to perform *ab initio* calculations for these systems, since no real peculiarity is expected.

Conclusion

The present study does confirm that Schiff-base heterodinuclear Ni–Ln complexes are soluble and stable in aqueous solution. Indeed, recrystallization under such conditions yields again a dinuclear Ni–Ln complex which differs from the initial complex by changes in the Ln coordination sphere. If the resulting complex is still coordinated to the four oxygen atoms of the outer coordination site of the Schiff base, two (out of the three) ancillary chelating nitrato ligands are replaced by three water molecules. This observation highlights the role of chelating nitrato anions in the nuclearity of Schiff base Ni–Ln complexes. The presence of only one chelating nitrato ligand is sufficient to impede an increase of the nuclearity of these complexes. But this condition is not sufficient; replacement of nitrato anions by chloride anions still leads to heterodinuclear Ni–Ln complexes with four ancillary water molecules in the Ln coordination sphere. This experimental result evidences the role of protic solvents, able to impede the coordination of a second NiL entity in the Ln coordination sphere. In contrast, the use of lanthanide salts soluble in non-protic solvents allows the isolation of trinuclear and cationic $[LNi–Ln–NiL]^{3+}$ complexes. A supplementary synthetic step can also be overtaken once we know that heterodinuclear Ni–Ln complexes are stable in solution. The reaction of a Ni–Ln complex soluble in a non-protic solvent with a LM complex (M = Cu, Zn) yields a heterotrinuclear complex made of three different metal ions, two different 3d ions and one 4f one. Applying this synthetic strategy to the use of metallocyanate entities should allow the preparation of complexes involving four different metal ions. Forthcoming work will be directed in that way. Furthermore we demonstrate that the lengthening of the axial bonds in the nickel coordination sphere, by replacement of water molecules by chloride ligands, induces a net increase of the positive zero-field splitting parameter *D*, which is also supported by *ab initio* calculations. Although large-spin ground states are expected in the trinuclear complexes (due to ferromagnetic Ni–Tb, Ni–Dy, and Ni–Gd interactions), a uniaxial and negative magnetoanisotropy is not present, with micro-SQUID measurements confirming a collapse of the hysteresis loops at zero-field.

Conflicts of interest

There are no conflicts to declare.

Acknowledgements

This work was supported by the European Union sixth framework program NMP3-CT-2005-515767 entitled "MAGMANet:

Molecular Approach to Nanomagnets and Multifunctional Materials".

References

1 J. P. Costes, F. Dahan, A. Dupuis and J. P. Laurent, *Inorg. Chem.*, 1997, **36**, 4884–4886.

2 (*a*) S. Biswas, J. Goura, S. Das, C. V. Topping, J. Brambleby, P. A. Goddard and V. Chandrasekhar, *Inorg. Chem.*, 2016, **55**, 8422–8436; (*b*) S. Y. Im, S. J. Park, H. J. Im and S. W. Lee, *Polyhedron*, 2016, **117**, 231–243; (*c*) S. K. Singh, M. F. Beg and G. Rajaraman, *Chem. – Eur. J.*, 2016, **22**, 672–680; (*d*) B. Cristovao, B. Miroslaw, J. Klak and M. Rams, *Polyhedron*, 2015, **85**, 697–704; (*e*) N. Ahmed, C. Das, S. Vaidya, S. K. Langley, K. S. Murray and M. Shanmugam, *Chem. – Eur. J.*, 2014, **20**, 14235–14239; (*f*) S. Das, S. Hossain, A. Dey, S. Biswas, E. Pardo, F. Lloret and V. Chandrasekhar, *Eur. J. Inorg. Chem.*, 2014, 3393–3400; (*g*) S. Sakamoto, T. Fujinami, K. Nishi, N. Matsumoto, N. Mochida, T. Ishida, Y. Sunatsuki and N. Re, *Inorg. Chem.*, 2013, **52**, 7218–7229; (*h*) M. Towatari, K. Nishi, T. Fujinami, N. Matsumoto, Y. Sunatsuki, M. Kojima, N. Mochida, T. Ishida, N. Re and J. Mrozinski, *Inorg. Chem.*, 2013, **52**, 6160–6178; (*i*) E. Cremades, S. Gómez-Coca, D. Aravena, S. Alvarez and E. Ruiz, *J. Am. Chem. Soc.*, 2012, **134**, 10532–10542; (*j*) S. Sakamoto, S. Yamauchi, H. Hagiwara, N. Matsumoto, Y. Sunatsuki and N. Re, *Inorg. Chem. Commun.*, 2012, **26**, 20–23; (*k*) F. Cimpoesu, F. Dahan, S. Ladeira, M. Ferbinteanu and J. P. Costes, *Inorg. Chem.*, 2012, **51**, 11279–11293; (*l*) K. C. Mondal, G. E. Kostakis, Y. Lan, W. Wernsdorfer, C. E. Anson and A. K. Powell, *Inorg. Chem.*, 2011, **50**, 11604–11611; (*m*) R. Maurice, L. Vendier and J. P. Costes, *Inorg. Chem.*, 2011, **50**, 11075–11081; (*n*) S. K. Sing, N. K. Tibrewal and G. Rajaraman, *Dalton Trans.*, 2011, **40**, 10897–10906; (*o*) J. P. Sutter, S. Dhers, R. Rajamani, S. Ramasesha, J. P. Costes, C. Duhayon and L. Vendier, *Inorg. Chem.*, 2009, **48**, 5820–5828; (*p*) J. P. Costes, T. Yamaguchi, M. Kojima and L. Vendier, *Inorg. Chem.*, 2009, **48**, 5555–5561; (*q*) S. Dhers, S. Sahoo, J. P. Costes, C. Duhayon, S. Ramasesha and J. P. Sutter, *CrystEngComm*, 2009, **11**, 2078–2083.

3 V. Chandrasekhar, B. M. Pandian, R. Boomishankar, A. Steiner, J. J. Vittal, A. Houri and R. Clérac, *Inorg. Chem.*, 2008, **47**, 4918–4929.

4 (*a*) T. D. Pasatoiu, A. Ghirri, A. M. Madalan, M. Affronte and M. Andruh, *Dalton Trans.*, 2014, **43**, 9136–9142; (*b*) A. Upadhyay, N. Komatireddy, A. Ghirri, F. Tuna, S. K. Langley, A. K. Srivastava, E. C. Sanudo, B. Moubaraki, K. S. Murray, E. J. L. McInnes, M. Affronte and M. Shanmugam, *Dalton Trans.*, 2014, **43**, 259–266; (*c*) A. Okazawa, T. Shimada, N. Kojima, S. Yoshii, H. Nojiri and T. Ishida, *Inorg. Chem.*, 2013, **52**, 13351–13355; (*d*) Z.-S. Meng, F.-S. Guo, J.-L. Liu, J.-D. Leng and M.-L. Tong, *Dalton Trans.*, 2012, **41**, 2320–2329; (*e*) A. S. R. Chesman, D. R. Turner, B. Moubaraki, K. S. Murray, G. B. Deacon and S. R. Batten, *Inorg. Chim. Acta*, 2012, **389**, 99–106; (*f*) H. Ke, L. Zhao, Y. Guo and J. Tang, *Inorg. Chem.*, 2012, **51**, 2699–2705; (*g*) J.-B. Peng, Q.-C. Zhang, X.-J. Kong, Y.-Z. Zheng, Y.-P. Ren, L.-S. Long, R.-B. Huang, L.-S. Zheng and Z. Zheng, *J. Am. Chem. Soc.*, 2012, **134**, 3314–3317; (*h*) E. Colacio, J. Ruiz, A. J. Mota, M. A. Palacios, E. Cremades, E. Ruiz, F. J. White and E. K. Brechin, *Inorg. Chem.*, 2012, **51**, 5857–5868; (*i*) H. Ke, L. Zhao, Y. Guo and J. Tang, *Inorg. Chem.*, 2012, **51**, 2699–2705; (*j*) Y. Gao, L. Zhao, X. Xu, G. F. Xu, Y. N. Guo, J. Tang and Z. Liu, *Inorg. Chem.*, 2011, **50**, 1304–1308; (*k*) E. Colacio, J. Ruiz-Sanchez, F. J. White and E. K. Brechin, *Inorg. Chem.*, 2011, **50**, 7268–7273; (*l*) C. G. Efthymiou, T. C. Stamatatos, C. Papatriantafyllopoulou, A. J. Tasiopoulos, W. Wernsdorfer, S. P. Perlepes and G. Christou, *Inorg. Chem.*, 2010, **49**, 9737–9739; (*m*) A. N. Georgopoulou, R. Adam, C. P. Raptopoulou, V. Psycharis, R. Ballesteros, B. Abarca and A. K. Boudalis, *Dalton Trans.*, 2010, **39**, 5020–5027.

5 J. P. Costes, B. Donnadieu, R. Gheorghe, G. Novitchi, J. P. Tuchagues and L. Vendier, *Eur. J. Inorg. Chem.*, 2008, 5235–5244.

6 J. P. Costes, F. Dahan and W. Wernsdorfer, *Inorg. Chem.*, 2006, **45**, 5–7.

7 J. P. Costes, F. Dahan, A. Dupuis and J. P. Laurent, *Inorg. Chem.*, 1997, **36**, 3429–3433.

8 P. Pascal, *Ann. Chim. Phys.*, 1910, **19**, 5–70.

9 A. K. Boudalis, J.-M. Clemente-Juan, F. Dahan and J. P. Tuchagues, *Inorg. Chem.*, 2004, **43**, 1574–1586.

10 J. J. Borrás-Almenar, J. M. Clemente-Juan, E. Coronado and B. S. Tsukerblat, *Inorg. Chem.*, 1999, **38**, 6081–6088; J. J. Borrás-Almenar, J. M. Clemente-Juan, E. Coronado and B. S. Tsukerblat, *J. Comput. Chem.*, 2001, **22**, 985–991.

11 F. James and M. Roos, *MINUIT Program*, a System for Function Minimization and Analysis of the Parameters Errors and Correlations, *Comput. Phys. Commun.*, 1975, **10**, 343–367.

12 SIR92 - A program for crystal structure solution. A. Altomare, G. Cascarano, C. Giacovazzo and A. Guagliardi, *J. Appl. Crystallogr.*, 1993, **26**, 343–350.

13 G. M. Sheldrick, *SHELX97 [Includes SHELXS97, SHELXL97, CIFTAB] - Programs for Crystal Structure Analysis (Release 97-2)*, Institüt für Anorganische Chemie der Universität, Tammanstrasse 4, D-3400 Göttingen, Germany, 1998.

14 WINGX - 1.63 Integrated System of Windows Programs for the Solution, Refinement and Analysis of Single Crystal X-Ray Diffraction Data. L. Farrugia, *J. Appl. Crystallogr.*, 1999, **32**, 837–838.

15 *International tables for X-Ray crystallography*, Kynoch press, Birmingham, England, 1974, vol. **IV**.

16 ORTEP32 for Windows. L. Farrugia, *J. Appl. Crystallogr.*, 1997, **30**, 565–568.

17 F. Neese, *ORCA-An ab initio, density functional and semiempirical program package v.3.0.1*, Max-Planck-Institut für Bioanorganische Chemie, Mülheim an der Ruhr, 2013.

18 J. P. Costes, R. Maurice and L. Vendier, *Chem. – Eur. J.*, 2012, **18**, 4031–4040.

19 B. O. Roos and P. Å. Malmqvist, *Phys. Chem. Chem. Phys.*, 2004, **6**, 2919–2927.

20 (*a*) B. A. Heß, C. M. Marian, U. Wahlgren and O. Gropen, *Chem. Phys. Lett.*, 1996, **251**, 365–371; (*b*) F. Neese, *J. Chem. Phys.*, 2005, **122**, 034107.

21 (*a*) C. Angeli, R. Cimiraglia and J.-P. Malrieu, *Chem. Phys. Lett.*, 2001, **350**, 297–305; (*b*) C. Angeli, R. Cimiraglia and J.-P. Malrieu, *J. Chem. Phys.*, 2002, **117**, 9138–9153; (*c*) C. Angeli, M. Pastore and R. Cimiraglia, *Theor. Chem. Acc.*, 2007, **117**, 743–754.

22 C. Bloch, *Nucl. Phys.*, 1958, **6**, 329–347.

23 J. Des Cloizeaux, *Nucl. Phys.*, 1960, **20**, 321–346.

24 R. Maurice, R. Bastardis, C. de Graaf, N. Suaud, T. Mallah and N. Guihéry, *J. Chem. Theory Comput.*, 2009, **5**, 2977–2984.

25 R. Maurice, C. de Graaf and N. Guihéry, *Phys. Chem. Chem. Phys.*, 2013, **15**, 18784–18804.

26 R. Maurice, R. Broer, N. Guihéry and C. de Graaf, Zero-field splitting in transition metal complexes: Ab initio calculations, effective Hamiltonians, model Hamiltonians, and crystal-field models, in *Handbook of Relativistic Quantum Chemistry*, ed. W. Liu, Springer-Verlag Berlin Heidelberg, 2017, pp. 765–796.

27 F. Weigend and R. Ahlrichs, *Phys. Chem. Chem. Phys.*, 2005, **7**, 3297–3305.

28 M. Llunell, D. Casanova, J. Cirera, J. M. Bofill, P. Alemany, S. Alvarez, M. Pinsky and D. Avnir, *SHAPE, v1.1b*, University of Barcelona, Barcelona, Spain, 2005.

29 J. P. Costes, F. Dahan, A. Dupuis and J. P. Laurent, *Inorg. Chem.*, 1996, **35**, 2400–2402.

30 W. Wernsdorfer, *Adv. Chem. Phys.*, 2001, **118**, 99–190.

31 A. M. Madalan, N. Avarvari and M. Andruh, *New J. Chem.*, 2006, **30**, 521–523.

32 J. P. Costes, S. Titos-Padilla, I. Oyarzabal, T. Gupta, C. Duhayon, G. Rajaraman and E. Colacio, *Chem. – Eur. J.*, 2015, **21**, 15785–15796.

33 S. Dhers, J. P. Costes, P. Guionneau, C. Paulsen, L. Vendier and J. P. Sutter, *Chem. Commun.*, 2015, **51**, 7875–7878.

34 M. Andruh, J. P. Costes, C. Diaz and S. Gao, *Inorg. Chem.*, 2009, **48**, 3342–3359.

35 A. Abragam and B. Bleaney, *Electron Paramagnetic Resonance of Transition ions*, Dover Publications, Dover, NY, 1986.

36 N. A. Bogdanov, R. Maurice, I. Rousochatzakis, J. van den Brink and L. Hozoi, *Phys. Rev. Lett.*, 2013, **110**, 127206.

37 (*a*) S. K. Singh, T. Gupta, P. Badkur and G. Rajaraman, *Chem. – Eur. J.*, 2014, **20**, 10305–10313; (*b*) S. Gómez-Coca, E. Cremades, N. Aliaga-Alcalde and E. Ruiz, *Inorg. Chem.*, 2014, **53**, 676–678; (*c*) I. Nemec, R. Herchel, I. Svoboda, R. Boca and Z. Travnicek, *Dalton Trans.*, 2015, **44**, 9551–9560; (*d*) M. Gruden-Pavlovic, M. Peric, M. Zlatarb and P. Garcia-Fernandez, *Chem. Sci.*, 2014, **5**, 1453–1462; (*e*) R. Ruamps, R. Maurice, C. de Graaf and N. Guihéry, *Inorg. Chem.*, 2014, **53**, 4508–4516; (*f*) J. N. Rebilly, G. Charron, E. Rivière, R. Guillot, A. L. Barra, M. D. Serrano, J. van Slageren and T. Mallah, *Chem. – Eur. J.*, 2008, **14**, 1169–1177.